

AnomalyControl: Learning Cross-modal Semantic Features for Controllable Anomaly Synthesis

Shidan He

Sun Yat-sen University
Tencent, WeChat Pay
Shenzhen, China

Bo Wang

Tencent, WeChat Pay
Shenzhen, China

Lei Liu

CUHK-Shenzhen
Ant Group
Hangzhou, China

Xiujun Shu

Tencent, WeChat Pay
Shenzhen, China

Shen Zhao*

Sun Yat-sen University
Shenzhen, China

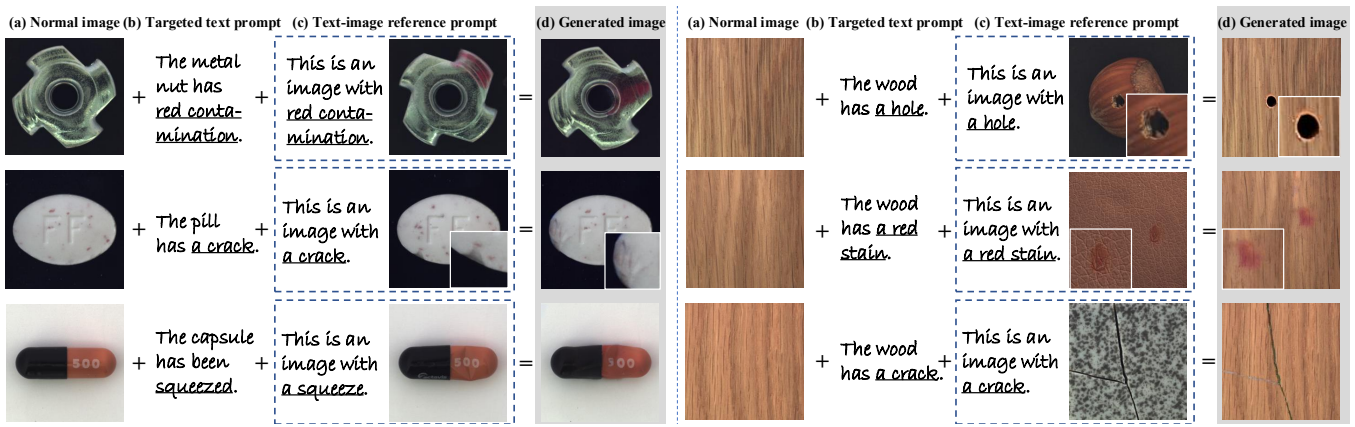


Figure 1: Our method learns cross-modal semantic features as the priors to achieve both **realism** and **generalization** for controllable anomaly synthesis. **Realism:** The targeted text prompt provides a full description for the targeted anomaly image (e.g., color, texture, and shape), while the text-image reference prompt provides a template for the targeted anomaly region (e.g., magnified area). **Generalization:** The text-image reference can exhibit a different material surface compared with the targeted text prompt (e.g., the right examples).

Abstract

Anomaly synthesis is a crucial approach to augment abnormal data for advancing anomaly inspection. Based on the knowledge learned from the large-scale pre-training, existing text-to-image anomaly synthesis methods predominantly focus on textual information or coarse-aligned visual features to guide the entire generation process. However, these methods often lack sufficient descriptors to capture the complicated characteristics of realistic anomalies (e.g., the fine-grained visual pattern of anomalies), limiting the realism and generalization of the generation process. To this end, we propose a novel anomaly synthesis framework called AnomalyControl to learn cross-modal semantic features as guidance signals, which could encode the generalized anomaly cues from text-image reference prompts and improve the realism of synthesized abnormal samples. Specifically, AnomalyControl adopts a flexible and non-matching prompt pair (*i.e.*, a text-image reference prompt and a targeted text prompt)¹, where a Cross-modal Semantic Modeling (CSM) module is designed to extract cross-modal semantic

features from the textual and visual descriptors. Then, an Anomaly-Semantic Enhanced Attention (ASEA) mechanism is formulated to allow CSM to focus on the specific visual patterns of the anomaly, thus enhancing the realism and contextual relevance of the generated anomaly features. Treating cross-modal semantic features as the prior, a Semantic Guided Adapter (SGA) is designed to encode effective guidance signals for the adequate and controllable synthesis process. Extensive experiments indicate that AnomalyControl can achieve state-of-the-art results in anomaly synthesis compared with existing methods while exhibiting superior performance for downstream tasks.

CCS Concepts

- Computing methodologies → Computer vision representations.

Keywords

Anomaly Synthesis, Controllable Generation, Text-to-Image Diffusion Models

*Corresponding author is Shen Zhao (e-mail: zhaosh35@mail.sysu.edu.cn).

¹Non-matching: the text-image reference prompt and targeted text prompt are only required to describe the same anomaly type without needing to match in surface details or materials.

1 Introduction

Anomaly inspection plays a crucial role in various fields, from industrial anomaly detection [16, 36] to medical imaging [12]. One of the most challenging issues is the scarcity of diverse abnormal data due to the resource-intensive procedure for acquiring large and varied datasets. Therefore, anomaly synthesis task [5, 6, 8, 10, 11, 19, 20, 32, 33, 38] gradually emerged as an advancing technique to improve the data scale of the available abnormal sample.

Many downstream tasks, such as anomaly detection and localization, could benefit from enriching the training dataset using synthetic anomaly samples. Recently, text-to-image synthesis techniques [24, 29] have received more research attention for their outperforming performance, which can generate visually realistic natural images according to the input text prompt. However, for the anomaly synthesis task, they still suffer from insufficient descriptors of the textual prompt, resulting in unsatisfactory realism for the generated anomalies. This limitation hampers the model's ability to recognize rare or previously unseen defect types.

Motivated by the success of publicly available large text-to-image diffusion models [1, 18, 25, 27, 30], many approaches proposed to incorporate extra control signals to assist the diffusion process, which could enrich the targeted text prompt via injecting more prior information. For example, ControlNet [35], Uni-ControlNet [37], and IP-Adapter [31] proposed to apply adapters on stable diffusion models [25] to provide extra control for generation. The main idea is to learn stylistic information from a reference image (called image prompt). However, image prompts without a clear focal point generally offer weak alignment signals, limiting the effectiveness of generating high-fidelity and customized images. This limitation is especially pronounced in anomaly synthesis tasks, where anomalies typically occupy only a small region of the image and can easily be overlooked during generation. As a result, the synthesized anomalies often lack sufficient details to match real samples, failing to meet the high precision required for effective anomaly inspection and resulting in a lack of realism in the synthesized samples.

To this end, this work aims to enhance the controllability of anomaly synthesis, improving the realism of synthesized samples and supporting more flexible and generalizable prompts. The resulting framework is called AnomalyControl (as shown in Figure 2). Specifically, the controllability signals come from a non-matching pair, *i.e.*, a text-image reference prompt, and a targeted text prompt. The text-image reference prompt includes a textual anomaly descriptor and visual anomaly descriptor, which are used to offer semantic and contextual cues for guiding the synthesis process. Importantly, the anomaly described by the text-image reference prompt is aligned with that indicated in the targeted text prompt, while the background and other properties are left unrestricted, allowing for greater flexibility in anomaly placement. To improve realism, we introduce Cross-modal Semantic Modeling (CSM) to capture cross-modal semantic features via multimodal interactions, where the Anomaly-Semantic Enhanced Attention (ASEA) mechanism could extract fine-grained information related to the anomaly region. By taking cross-modal semantic features as the prior, the Semantic Guided Adapter (SGA) could insert effective semantic signals to support an adequate and controllable synthesis process. Table 1 makes a comparison between AnomalyControl and previous

methods, where our method exhibits several advantages in four aspects: 1) Realism: Our model generates highly realistic anomalies by using cross-modal semantic features, closely matching real-world defects. 2) Generalization: Synthesizes diverse anomalies beyond the training distribution, improving adaptability to unseen cases. 3) Plug-and-Play: The Semantic Guided Adapter (SGA) allows flexible anomaly synthesis without retraining the diffusion model, making it efficient and scalable. 4) Controllability: AnomalyControl provides precise control over anomaly types and placements using text-image reference and targeted text prompts.

In summary, our contributions are as follows:

- A novel framework called AnomalyControl is proposed to achieve controllable anomaly synthesis in a flexible manner, which can generate realistic and generalized anomaly samples guided by a non-matching pair.
- We design a Cross-modal Semantic Modeling (CSM) module to extract cross-modal semantic features from the textual and visual anomaly descriptors, where an Anomaly-Semantic Enhanced Attention (ASEA) mechanism can encode fine-grained visual details into cross-modal semantic features via multimodal interactions, which could further improve the realism of generated anomalies.
- We formulate a Semantic Guided Adapter (SGA) allowing cross-modal semantic features to pass through the generation procedure (*i.e.*, diffusion process), providing adequate and controllable synthesis instructions to generate high-quality anomalies.
- Extensive experiments demonstrate that our method can generate realistic and generalized anomalies based on different control signals (as shown in Figure 1) and significantly enhance anomaly inspection performance.

2 Related Work

2.1 Anomaly Synthesis

Anomaly synthesis has become an essential technique to support anomaly detection systems, especially in scenarios where real defect data is scarce. Existing methods can be broadly divided into two main categories. First, crop-and-paste anomaly augmentation methods [5, 32] combine normal images with abnormal patterns sourced from small abnormal samples or external textures. While these methods are computationally efficient and straightforward to implement, they often lack realism and generalization, limiting their ability to represent the complex characteristics of anomalies. Second, generative model-based methods [6, 8, 10, 11, 19, 20, 33, 38], such as GANs and diffusion models, generate anomalies from scratch or by fine-tuning pre-trained models. Although these methods typically perform well for in-distribution anomalies, they require sufficient sample generalization and frequently struggle to produce out-of-distribution anomalies, which limits their ability to generalize to unseen defect types.

2.2 Text-to-Image Diffusion Models

Since fine-tuning large pre-trained models is often inefficient, using adapters has become a more efficient alternative. Adapters introduce a small number of trainable parameters into the original model while freezing the pre-trained weights, significantly reducing training costs. With the success of large text-to-image diffusion models

Table 1: Comparisons with previous methods. Our AnomalyControl can perform well for realism and generalization, along with plug-and-play flexibility and controllability. **Realism** refers to the ability to generate realistic anomaly images with complex and fine-grained details. **Generalization** indicates the capability to transfer anomaly features across different objects and surfaces, allowing the model to generate diverse anomalies beyond the pre-training knowledge. **The generalization ability of previous anomaly synthesis methods is limited by the pre-training knowledge due to lacking large-scale high-fidelity anomaly data. Large-scale pre-training on natural images can improve the generalization ability of natural image generation methods, but they still suffer from low-quality anomaly synthesis due to the complicated characteristics of anomalies.**

Method	Venue	Task	Realism	Generalization	Plug-and-Play	Controllability
DRAEM [32]	ICCV'21	Anomaly Synthesis			✓	
DefGAN [33]	WACV'21	Anomaly Synthesis	✓			
DFMGAN [6]	AAAI'23	Anomaly Synthesis	✓			
AnoDiff [11]	AAAI'24	Anomaly Synthesis	✓			
ControlNet [35]	ICCV'23	Image Generation		✓	✓	✓
Uni-ControlNet [37]	NeurIPS'23	Image Generation		✓	✓	✓
IP-Adapter [31]	Arxiv'23	Image Generation		✓	✓	✓
AnomalyControl		Anomaly Synthesis	✓	✓	✓	✓

like DALL-E 2 [24], Imagen [27], and Stable Diffusion [25], significant progress has been made in image generation. However, writing complex text prompts remains a challenge, and pure text often fails to fully express complex scenes or concepts. To address this, methods such as ControlNet [35] and Uni-ControlNet [37] have introduced lightweight adapters in pre-trained Stable Diffusion models, enabling more precise control by incorporating additional prompts, such as structural or image-based control. IP-Adapter [31] further optimizes this approach by introducing a decoupled cross-attention mechanism, improving the effectiveness of image prompting, and even achieving performance comparable to fine-tuning the entire model. However, image prompts without a clear focus often provide weak alignment signals, making it difficult to generate high-fidelity, customized images, especially in anomaly synthesis, where anomalies are small and easily overlooked.

3 Methods

3.1 Preliminaries

Stable Diffusion. Our method is built upon Stable Diffusion [25], which efficiently performs the diffusion process in a low-dimensional latent space instead of pixel space using an auto-encoder [14]. Specifically, given an input $x_i \in \mathbb{R}^{H \times W \times 3}$, the encoder maps it to a latent representation $z_0 = \xi(x_i)$, where $z_0 \in \mathbb{R}^{h \times w \times c}$ with $H/h = W/w$ as the downsampling factor and c as the number of latent dimensions. The diffusion process utilizes a denoising UNet [26] to gradually refine a noisy latent z_t , conditioned on the current timestep T and a textual prompt embedding C . C represents the embedding of the targeted text prompt, generated by a pre-trained CLIP [23] text encoder. The training objective is defined as:

$$\mathcal{L} = \mathbb{E}_{z_t, t, C, \epsilon \sim \mathcal{N}(0, 1)} [\|\epsilon - \epsilon_\theta(z_t, t, C)\|_2^2], \quad (1)$$

where the goal is to predict and remove the noise ϵ added to z_t at each timestep.

Overall Framework. The pipeline of AnomalyControl is illustrated in Figure 2. Our framework consists of two main modules: Cross-modal Semantic Modeling (CSM) and Semantic Guided Adapter (SGA). Given the text-image reference prompts as the input,

i.e., a visual anomaly descriptor I_a and textual anomaly descriptor T_a as the reference, CSM module aims to extract fine-grained cross-modal semantic features by integrating both text and image information using a vision-language model (VLM). An Anomaly-Semantic Enhanced Attention (ASEA) is introduced to refine the attention process in VLM, ensuring that the model can focus on the specific visual patterns of the anomaly, thus enhancing the realism and contextual relevance of the generated anomaly features. The SGA then introduces these enriched cross-modal semantic features as priors into the diffusion process, allowing flexible control over anomaly characteristics. Together, these components ensure that generated anomalies are realistic and contextually aligned with descriptive cues. The detailed training algorithm of our AnomalyControl is outlined in Algorithm 1.

3.2 AnomalyControl

3.2.1 Cross-modal Semantic Modeling. Leveraging the text-image reference prompt, the CSM module targets to encode sufficient cross-modal reference information as control signals for the diffusion process, *i.e.*, consistent anomaly semantics from the text-image prompt.

Specifically, the text-image reference prompt provides a visual anomaly descriptor I_a and a textual anomaly descriptor T_a . Note that such text-image reference prompt only focuses on the contextual and descriptive information of the anomaly region, excluding the anomaly-unrelated information, such as background and materials. Such a pattern would allow greater flexibility in anomaly placement. In detail, I_a defines a specific anomaly pattern to provide a direct visual context reference, ensuring accurate visual control over the generated anomaly. T_a is created by combining an anomaly-specific keyword K with a template, providing semantic guidance to help the model generate samples that accurately reflect the designated anomaly type and attributes. The anomaly described in the T_a aligns with the anomaly region in the I_a , while the background and other elements of I_a remain unconstrained.

To capture effective cross-modal information from the text-image reference, a frozen VLM with cross-attention layers is utilized for

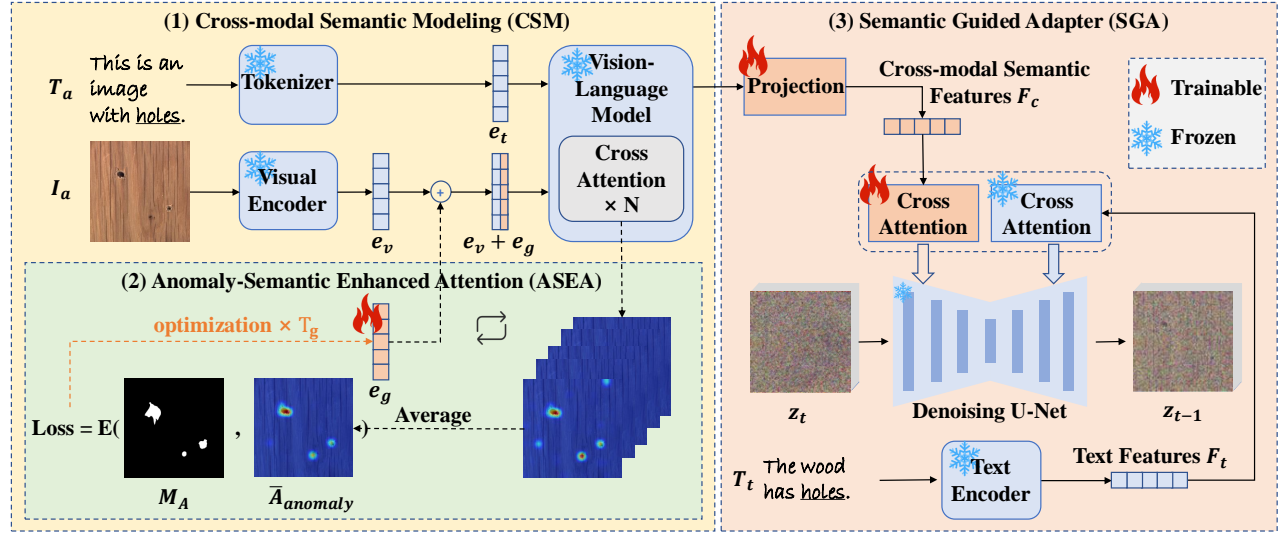


Figure 2: Overall pipeline of the proposed AnomalyControl. Our framework consists of three main modules to enhance controllability in anomaly synthesis. (1) Cross-modal Semantic Modeling (CSM) integrates both visual anomaly descriptors I_a and textual anomaly descriptors T_a to capture precise cross-modal semantic features using a frozen vision-language model (VLM). (2) Anomaly-Semantic Enhanced Attention (ASEA) employ a trainable attention guidance variable e_g to emphasize the designated anomaly regions, which can capture more accurate semantic information without retraining the frozen VLM. (3) Semantic Guided Adapter (SGA) utilizes a decoupled cross-attention to support controllable anomaly synthesis, allowing for a flexible and generalized generation.

its powerful multimodal integration ability. Thus, VLM-based CSM could integrate the reference image and text to obtain a unified semantic feature for the anomaly, called a cross-modal semantic feature, which serves as a prior for the following diffusion process. Natural needs arise from the anomaly-specific regions without losing fine-grained detail to generate realistic and contextually accurate anomalies, which motivates the introduction of the ASEA mechanism in the following section.

3.2.2 Anomaly-Semantic Enhanced Attention. ASEA forces the CSM’s attention to focus on designated anomaly regions within the image reference, enabling precise extraction of anomaly-specific features for high-fidelity synthesis. The main pathway is to isolate the anomaly region in the attention map and optimize a trainable attention guidance variable, e_g , which assists the frozen VLM in prioritizing relevant anomaly areas without retraining steps.

The textual anomaly descriptor T_a is structured as the template of “*This is an image with [anomaly]*”, where the variable *[anomaly]* specifies the anomaly type. L_{prefix} represents the length of the fixed prefix “*This is an image with*”. L denotes the total length of T_a . The anomaly descriptor *[anomaly]* begins at position $L_{\text{prefix}} + 1$ and extends to L .

Firstly, an attention map A is generated by the VLM’s cross-attention layer, focusing on the feature span A_{anomaly} associated with the *[anomaly]* part of the text prompt. A_{anomaly} captures the anomaly-specific attention values: $A_{\text{anomaly}} = A[L_{\text{prefix}} + 1 : L, :]$. By averaging these values across the anomaly section, we compute a mean attention map, \bar{A}_{anomaly} , which helps stabilize the focus by

reducing noise from individual tokens:

$$\bar{A}_{\text{anomaly}} = \frac{1}{L - L_{\text{prefix}}} \sum_{i=L_{\text{prefix}}+1}^L A[i, :], \quad (2)$$

To further refine the attention on anomaly regions, we apply an anomaly region mask M_A to \bar{A}_{anomaly} . This mask constrains attention to the spatial area of interest in the image, which is enhanced by introducing the trainable attention guidance variable e_g . The optimization of e_g is guided by an energy function [4], defined as:

$$E(\bar{A}_{\text{anomaly}}, M_A) = \left(1 - \frac{\sum_{i \in M_A} \bar{A}_{\text{anomaly},i}}{\sum_i \bar{A}_{\text{anomaly},i}} \right)^2, \quad (3)$$

where $i \in M_A$ refers to indices within the masked region. This function encourages concentration within M_A , prioritizing relevant features in the anomaly area.

Finally, e_g is optimized iteratively over T_g steps using gradient descent to minimize the energy function:

$$e_g \leftarrow e_g - \alpha \nabla_{e_g} E(\bar{A}_{\text{anomaly}}, M_A), \quad (4)$$

where α is the learning rate. Through this iterative refinement, ASEA aligns the model’s attention precisely with M_A , effectively capturing anomaly-specific details. The challenge here lies in maintaining focused attention on the anomaly regions without disrupting the model’s overall comprehension, a task ASEA addresses by carefully guiding attention with e_g .

3.2.3 Semantic Guided Adapter. Using solely image features as the prior [31, 37], previous approaches often miss critical details in subtle anomaly regions with low signal-to-noise ratios. Motivated

by this, SGA relies on a richer, semantically focused representation, *i.e.*, cross-modal semantic features produced by CSM, which captures fine-grained anomaly details essential for accurate synthesis. Concretely, based on the decoupled cross-attention [31], SGA introduces an adaptive mechanism to incorporate an additional targeted text prompt T_t as input.

To facilitate classifier-free guidance [9], similar to text conditioning, SGA employs random dropout during training. This process involves occasionally setting cross-modal semantic features to zero, allowing the model to jointly learn both conditional and unconditional prompts. The enhanced cross-attention mechanism for integrating text and cross-modal semantic features is defined as:

$$Z_{\text{new}} = \mathcal{S} \left(\frac{Q(K)^T}{\sqrt{d}} \right) V + \gamma \cdot \mathcal{S} \left(\frac{Q(K')^T}{\sqrt{d}} \right) V', \quad (5)$$

where γ is a weight to balance these two terms. \mathcal{S} is the function of Softmax. Q , K , and V are the query, key, and value matrices for the attention operation applied to text cross-attention, while K' and V' correspond to cross-modal attention. Given the query features Z and cross-modal semantic features F_c , the query matrix Q is defined as $Q = ZW_q$, with $K' = F_c W'_k$ and $V' = F_c W'_v$. Notably, only W'_k and W'_v are trainable parameters, focusing the adaptation on cross-modal information. During training, only the parameters of the SGA and e_g are optimized, while the pre-trained diffusion model and VLM parameters remain frozen. The entire AnomalyControl pipeline is trained on image-text pairs of anomaly images, with a training objective based on the original Stable Diffusion work:

$$\mathcal{L} = \mathbb{E}_{\epsilon \sim \mathcal{N}(0,1)} [\|\epsilon - \epsilon_\theta(\text{concat}(z_t, M_A, z_m), t, F_t, F_c)\|_2^2] \quad (6)$$

Here, z_m represents the masked image latent. This setup allows the SGA to integrate anomaly-specific semantic signals effectively, ensuring high-quality and controllable anomaly synthesis.

4 Experiments

4.1 Experimental setup

Datasets We conduct experiments on three datasets, including MVTec AD [2, 3], MPDD [13], and ViSA [39], to evaluate the performance of our method. We use the first one-third of the anomaly dataset IDs as the training set to train the anomaly synthesis model, with the remaining two-thirds used for testing. The anomaly synthesis model generates 1,000 pairs of anomaly images and corresponding masks for each anomaly category using normal data. The masks are generated using the mask generation method from AnoDiff [11]. These pairs of anomaly images and their corresponding masks, along with normal images from the training set, are then used to train downstream anomaly detection models, following the same approach as DRAEM [32] and AnoDiff [11].

Metrics. Inception Score (IS) [28] [11] is to evaluate the quality and diversity of synthesized anomalies. Intra-cluster Pairwise Learned Perceptual Image Patch Similarity (IC-LPIPS, abbreviated as IL) [21] is to evaluate perceptual similarity and the generalization of synthetic anomalies. For accuracy in downstream tasks such as anomaly detection and localization, we employed measurements through pixel-level and image-level Area Under the Receiver Operating Characteristic Curve (AUROC), Average Precision (AP), and F1-max scores.

Algorithm 1: AnomalyControl Training Algorithm

Data: Visual anomaly descriptor I_a , textual anomaly descriptor T_a , anomaly region mask M_A , targeted text prompt T_t , time steps T
Input: Number of training steps T_{train} , Guidance steps T_g
Output: Trained model parameters for AnomalyControl

```

for  $t_{\text{train}} \leftarrow 1$  to  $T_{\text{train}}$  do
  Sample a batch of images  $I$  from the training dataset  $I_a$ 
  Encode images to latent space:  $z = \text{Encoder}(I)$ 
  Sample noise  $\epsilon \sim \mathcal{N}(0, 1)$ 
  Sample time step  $t \sim \text{Uniform}(1, T)$ 
  Add noise to the latent variable  $z$  to obtain  $z_t$ 
  Set trainable attention guidance variable  $e_g = 0$ 
  Extract text embedding  $e_t$  and visual embedding  $e_v$  from the frozen VLM.
  for  $g \leftarrow 1$  to  $T_g$  do
    Generate attention map  $A = \text{VLM}_{\text{crossattn}}(e_t, e_v + e_g)$ 
    Compute average attention map  $\bar{A}_{\text{anomaly}}$  by Eq. 2
    Compute  $E(\bar{A}_{\text{anomaly}}, M_A)$  by Eq. 3
    Update  $e_g$  by Eq. 4
    Generate cross-modal semantic feature
     $F_c = \text{VLM}(e_t, e_v + e_g)$ 
    Compute loss  $\mathcal{L}$  by Eq. 6
    Backpropagate  $\mathcal{L}$  and update SGA parameters
  return Trained AnomalyControl model parameters

```

Implementation Details. AnomalyControl is implemented with the HuggingFace Diffusers library [22] and built on the Stable Diffusion 1.5 (SD1.5) model. The VLM utilized in CSM is based on BLIP-2 [15], which provides robust semantic feature extraction for cross-modal inputs. We incorporate a new cross-attention layer into each of SD1.5's 16 cross-attention layers, setting the cross-modal guidance strength parameter $\gamma = 1$ for balanced guidance. The number of guidance steps T_g in ASEA is set to 3. Additional details regarding the implementation are provided in Appendix A.

4.2 Comparison in Anomaly Synthesis

Table 2 illustrates the quantitative results for the generation task on the MVTec AD dataset. Our method achieves the highest average IS of 1.84 and the highest average IL of 0.35, surpassing all other methods in both overall quality and generalization. These results demonstrate our model's ability to generate high-quality, diverse anomalies that closely resemble real-world anomalies while maintaining robustness across different anomaly types.

Figure 3 displays the results of anomaly synthesis on 15 objects from the MVTec AD dataset. Our approach generates anomalies that are realistic and contextually consistent with the original images. For instance, in the hazelnut example, the generated anomaly of a cracked and broken shell is highly consistent with the texture and appearance of the original object, while maintaining a precise match with the defined mask area. Similarly, in the capsule and wood examples, our method accurately generates anomalies like incorrect imprints and scratches, showing its capability to faithfully replicate defects within the given context of the original image.

Table 2: Generation quantitative results with IS and IC-LPIPS (abbreviated as IL) on MVTec AD dataset. Bold indicates the best results, and underline indicates the second-best results. The results show that our method could obtain the SOTA results.

Method	Metric	bottle	cable	caps	carp	grid	hazel	leath	metal	pill	screw	tile	brush	trans	wood	zipper	Mean
DiffAug [38]	IS	1.59	1.72	1.34	1.19	1.96	1.67	2.07	1.58	1.53	1.10	1.93	1.33	1.34	2.05	1.30	1.58
	IL	0.03	0.07	0.03	0.06	0.06	0.05	0.06	0.29	0.05	0.10	0.09	0.06	0.05	0.30	0.05	0.09
CDC [20]	IS	1.52	1.97	1.37	1.25	1.97	1.97	1.80	1.55	1.56	1.13	2.10	1.63	1.61	2.05	1.30	1.65
	IL	0.04	0.19	0.06	0.03	0.07	0.05	0.07	0.04	0.06	0.11	0.12	0.06	0.13	0.03	0.05	0.07
SDGAN [19]	IS	1.57	1.89	1.49	1.18	1.95	1.85	2.04	1.45	1.61	1.17	<u>2.53</u>	1.78	1.76	2.12	1.25	1.71
	IL	0.06	0.19	0.03	0.11	0.10	0.16	0.12	0.28	0.07	0.10	0.21	0.03	0.13	0.25	0.10	0.13
DefGAN [33]	IS	1.39	1.70	1.59	<u>1.24</u>	2.01	1.87	2.12	1.47	1.61	1.19	2.35	1.85	1.47	2.19	1.25	1.69
	IL	0.07	0.22	0.04	0.12	0.12	0.19	0.14	0.30	0.10	0.12	0.22	0.03	0.13	0.29	0.10	0.15
DFMGAN [6]	IS	1.62	1.96	1.59	1.23	1.97	1.93	2.06	1.49	<u>1.63</u>	1.12	2.39	<u>1.82</u>	1.64	2.12	1.29	1.72
	IL	<u>0.12</u>	0.25	0.11	0.13	0.13	0.24	0.17	<u>0.32</u>	0.16	0.14	0.22	0.18	0.25	0.35	0.27	0.20
AnoDiff [11]	IS	1.58	<u>2.13</u>	<u>1.59</u>	1.16	<u>2.04</u>	2.13	1.94	<u>1.96</u>	1.61	1.28	<u>2.54</u>	1.68	1.57	<u>2.33</u>	<u>1.39</u>	1.80
	IL	0.19	<u>0.41</u>	0.21	<u>0.24</u>	<u>0.44</u>	<u>0.31</u>	<u>0.41</u>	0.30	<u>0.26</u>	0.30	<u>0.55</u>	<u>0.21</u>	<u>0.34</u>	<u>0.37</u>	0.25	<u>0.32</u>
Ours	IS	1.63	2.14	1.69	1.18	2.26	<u>2.12</u>	<u>2.08</u>	1.98	1.64	<u>1.25</u>	2.54	1.80	<u>1.66</u>	<u>2.20</u>	1.40	1.84
	IL	<u>0.19</u>	<u>0.44</u>	<u>0.20</u>	<u>0.28</u>	<u>0.47</u>	<u>0.35</u>	<u>0.43</u>	<u>0.34</u>	<u>0.27</u>	<u>0.28</u>	<u>0.53</u>	<u>0.24</u>	<u>0.39</u>	<u>0.40</u>	<u>0.26</u>	<u>0.35</u>

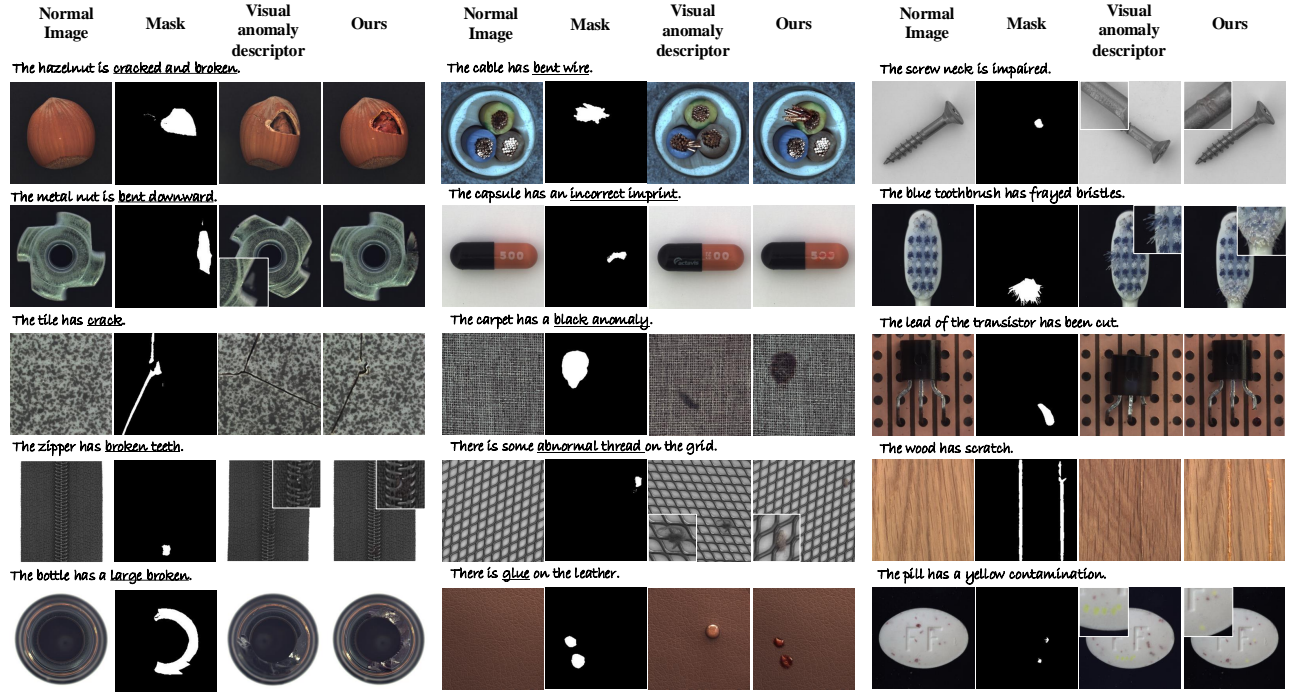
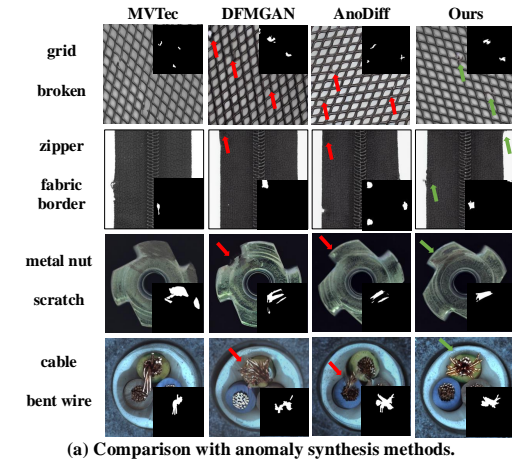


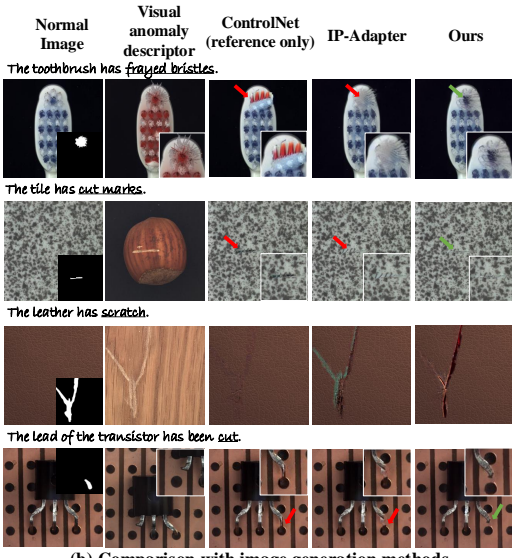
Figure 3: Display of anomaly synthesis on 15 objects from the MVTec AD dataset. The first column shows the normal image, the second column represents the mask area where anomalies need to be generated, the third column contains the visual anomaly descriptor providing visual guidance, and the fourth column displays the results generated by our method. Unlike simply copying the anomaly shown in the visual anomaly descriptor, our model predicts what the anomaly would look like in the given region indicated by the mask, considering the material and texture of the original normal image. The generated anomalies are consistent with the context of the image and are realistic in their appearance. Zoom in for better clarity and details.

Figure 4 provides a qualitative evaluation of our approach's effectiveness in anomaly synthesis. (a) In comparison with anomaly synthesis methods, our approach outperforms existing methods by producing anomalies with enhanced realism, closely aligning

with real-world defect patterns. For example, in the grid and cable examples, our method produces the clearest and most realistic anomalies, closely matching the texture and material of the original image. In contrast, other methods generate anomalies that lack fine detail or even introduce artifacts, resulting in noticeable ghosting



(a) Comparison with anomaly synthesis methods.



(b) Comparison with image generation methods.

Figure 4: Qualitative Evaluation. Our method could exhibit large improvements in realism and generalization. (a) **Comparison with anomaly synthesis methods.** Each row showcases anomalies across various object categories, where binary-value masks indicate the position of the generated anomaly regions. Our method excels in generating realistic anomalies in regions where other methods fail to capture fine details, resulting in unrealistic anomalies (e.g., DFMGAN, “metal nut”), artifacts (e.g., DFMGAN and AnoDiff, “cable”), or misaligned/fail to generate corresponding anomalies within the mask (e.g., DFMGAN and AnoDiff, “grid” and “zipper”). (b) **Comparison with image generation methods.** From left to right, the columns display a normal image with a target mask, a visual anomaly descriptor to provide visual guidance, and the generated results using different methods (i.e., reference-only mode ControlNet, IP-Adapter, and our method), respectively. Our method generates anomalies that are well-aligned with the visual cues in the descriptor, producing defects with a high degree of realism and relevance.

Table 3: Results of anomaly detection on three datasets. “-P” denotes the results of anomaly localization (pixel-level) and “-I” denote the results of anomaly detection (image-level). **Bold** values indicate the best results, and underlined values indicate the second-best results. Our method achieves state-of-the-art results in both anomaly detection and localization, surpassing other methods in most metrics across all three datasets.

MVTec AD						
Method	AUC-P	AP-P	F1-P	AUC-I	AP-I	F1-I
DRAEM [32]	92.2	54.1	53.1	94.6	97.0	94.4
PRN [34]	96.9	66.2	64.7	91.6	96.6	92.4
DFMGAN [6]	90.0	62.7	62.1	87.2	94.8	94.7
AnoDiff [11]	<u>99.1</u>	81.4	76.3	<u>99.2</u>	<u>99.7</u>	98.7
Ours	99.5	87.4	81.2	99.3	99.8	<u>98.0</u>
MPDD						
Method	AUC-P	AP-P	F1-P	AUC-I	AP-I	F1-I
DRAEM [32]	85.2	36.7	38.3	87.6	73.4	67.8
PRN [34]	90.7	40.8	41.5	86.3	77.6	76.3
DFMGAN [6]	92.4	41.6	45.5	92.5	78.5	78.9
AnoDiff [11]	<u>95.0</u>	47.6	<u>49.5</u>	<u>95.3</u>	<u>88.5</u>	<u>88.0</u>
Ours	96.5	50.6	51.2	98.4	90.5	89.1
VisA						
Method	AUC-P	AP-P	F1-P	AUC-I	AP-I	F1-I
DRAEM [32]	88.8	25.4	24.6	84.1	88.2	87.4
PRN [34]	87.0	20.8	21.5	80.5	81.9	82.3
DFMGAN [6]	95.2	39.9	40.2	87.1	85.2	85.7
AnoDiff [11]	<u>98.0</u>	<u>33.2</u>	<u>37.1</u>	<u>96.2</u>	<u>96.9</u>	<u>92.6</u>
Ours	99.0	42.5	48.0	96.8	97.2	93.5

or misalignment with the original context. (b) In the comparison with image generation methods, we selected reference images from different categories than the target images (for the first three rows) or from the same category with anomalies in different locations (for the fourth row). This setup demonstrates our method’s flexibility in transferring anomalies across various contexts and positions, thereby enhancing the model’s generalization capability. Our approach demonstrates superior control over anomaly placement and appearance, accurately capturing the characteristics of the reference anomalies. This improvement in visual fidelity highlights our method’s advantage in generating realistic, high-quality anomalies.

4.3 Comparison in Downstream Tasks

As shown in Table 3, our model consistently outperformed other anomaly synthesis methods across most evaluation metrics, demonstrating superior efficacy in both anomaly detection and localization. By enabling fine-grained controls over the appearance of anomalies, our approach can ensure that the generated samples closely resemble real-world defects. This capability is crucial in providing diverse and realistic training data, allowing downstream models to generalize better to real-world anomalies and improve both detection sensitivity and localization accuracy.

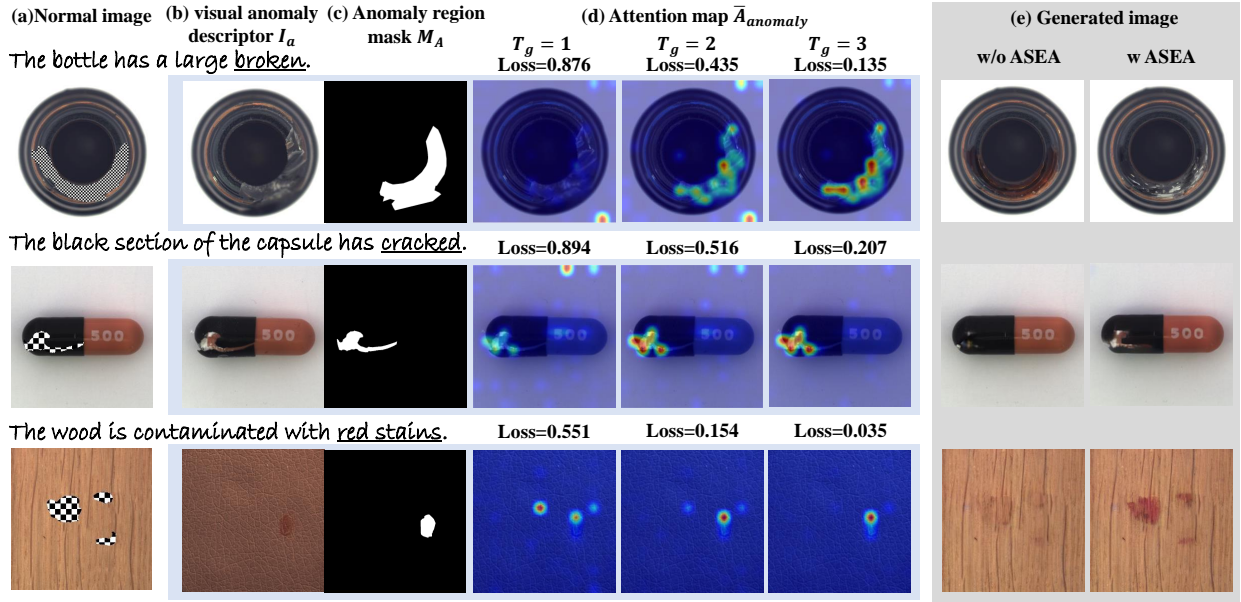


Figure 5: Effect of guidance steps T_g in ASEA. As T_g increases, the loss value is decreased, where ASEA progressively refines VLM’s attention on anomaly regions. The generated images exhibit improved anomaly realism, confirming the effectiveness of ASEA in focusing on specified anomaly regions and producing more visually realistic anomalies.

Table 4: Ablation Study on the MVTec-AD dataset. All modules (CSM, ASEA, and SGA) could improve the effectiveness of the method. We also study the impact of different guidance steps T_g in ASEA. **Bold** values indicate the best results, and underlined values indicate the second-best results. The results demonstrate the significant contributions of each module and the effectiveness of adjusting T_g for optimizing anomaly detection.

SGA	CSM	ASEA- T_g	IS	IL	AUC-P	AUC-I
-	-	-	1.50	0.18	90.3	93.0
✓	-	-	1.66	0.23	92.7	95.4
✓	✓	-	1.69	0.25	93.1	95.8
✓	✓	1	1.70	0.25	94.1	96.8
✓	✓	2	1.78	0.28	96.2	97.9
✓	✓	3	1.84	0.35	99.5	99.3
✓	✓	4	1.84	<u>0.33</u>	99.3	99.3
✓	✓	5	1.84	0.35	<u>99.4</u>	<u>99.0</u>

4.4 Ablation Study

From the experimental results in Table 4, it is observed that the stepwise introduction of each module significantly improves model performance. First, with only the SGA module, IS and IL increase to 1.66 and 0.23, respectively, while AUC-P and AUC-I reach 92.7 and 95.4. At this stage, the model only uses the visual anomaly descriptor, functioning as an adapter based solely on the image prompt. The addition of the SGA module shows that SGA can strengthen the focus on the anomaly regions in the image. When the CSM module is further introduced, IS rises from 1.66 to 1.69, IL from 0.23 to 0.25, and AUC-P and AUC-I reach 93.1 and 95.8. This improvement indicates that the CSM module incorporates the textual anomaly descriptor, integrating it with the visual anomaly descriptor for

cross-modal semantic fusion, thereby improving the quality and coherence of anomaly generation. As described in the methods section, the CSM module captures cross-modal semantic features of the anomaly region through multimodal interactions, resulting in anomaly features that align better with the intended descriptions. Finally, for the ASEA module, different guidance steps T_g demonstrate its impact on model performance. When $T_g = 3$, all metrics reach optimal values, providing the best balance between computational efficiency and performance. Increasing T_g to 4 or 5 shows marginal improvements, indicating that performance gains plateau while computational costs continue to rise. As shown in Figure 5, ASEA progressively refines VLM’s focus on specified anomaly areas, leading to generated images with higher anomaly realism. This indicates ASEA’s effectiveness in concentrating attention, resulting in visually realistic and detailed anomalies. By enhancing focus on anomaly-specific regions, ASEA effectively helps to generate high-quality, detailed anomaly images.

More experiments and discussions are provided in the Appendix.

5 Conclusion

In this paper, we propose an AnomalyControl framework for controllable anomaly synthesis, which enables the flexible generation of realistic and generalized anomaly samples. AnomalyControl introduces two three modules, *i.e.*, Cross-modal Semantic Modeling (CSM), Anomaly-Semantic Enhanced Attention (ASEA), and Semantic Guided Adapter (SGA). To enhance the realism of the synthesized anomalies, CSM aims to extract detailed cross-modal semantic features based on the textual and visual anomaly descriptors, where ASEA could capture fine-grained visual details through

multimodal interactions. Then, prompted by precise and controllable instructions, SGA could leverage these enriched semantic signals to guide the diffusion process for high-quality anomaly synthesis. Extensive experiments indicate that AnomalyControl can achieve state-of-the-art results in anomaly synthesis by generating realistic and generalized anomalies based on different control signals and outperforming existing methods for downstream tasks.

References

- [1] Yogesh Balaji, Seungjun Nah, Xun Huang, Arash Vahdat, Jiaming Song, Qinsheng Zhang, Karsten Kreis, Miika Aittala, Timo Aila, Samuli Laine, et al. 2022. ediff-i: Text-to-image diffusion models with an ensemble of expert denoisers. *arXiv preprint arXiv:2211.01324* (2022).
- [2] Paul Bergmann, Kilian Batzner, Michael Fauser, David Sattlegger, and Carsten Steger. 2021. The MVTec anomaly detection dataset: a comprehensive real-world dataset for unsupervised anomaly detection. *International Journal of Computer Vision (IJCV)* 129, 4 (2021), 1038–1059.
- [3] Paul Bergmann, Michael Fauser, David Sattlegger, and Carsten Steger. 2019. MVTec AD—A comprehensive real-world dataset for unsupervised anomaly detection. In *Proceedings of the IEEE/CVF Conference on Computer Vision and Pattern Recognition (CVPR)*. 9592–9600.
- [4] Minghao Chen, Iro Laina, and Andrea Vedaldi. 2024. Training-free layout control with cross-attention guidance. In *Proceedings of the IEEE/CVF Winter Conference on Applications of Computer Vision (WACV)*. 5343–5353.
- [5] Ruitao Chen, Guoyang Xie, Jiaqi Liu, Jinbao Wang, Ziqi Luo, Jinfan Wang, and Feng Zheng. 2023. Easynet: An easy network for 3d industrial anomaly detection. In *Proceedings of the 31st ACM International Conference on Multimedia (ACM MM)*. 7038–7046.
- [6] Yuxuan Duan, Yan Hong, Li Niu, and Liqing Zhang. 2023. Few-shot defect image generation via defect-aware feature manipulation. In *Proceedings of the AAAI Conference on Artificial Intelligence (AAAI)*, Vol. 37. 571–578.
- [7] Rinon Gal, Yuval Alaluf, Yuval Atzmon, Or Patashnik, Amit H Bermano, Gal Chechik, and Daniel Cohen-Or. 2022. An image is worth one word: Personalizing text-to-image generation using textual inversion. *arXiv preprint arXiv:2208.01618* (2022).
- [8] Guan Gui, Bin-Bin Gao, Jun Liu, Chengjie Wang, and Yunsheng Wu. 2024. Few-Shot Anomaly-Driven Generation for Anomaly Classification and Segmentation. In *European Conference on Computer Vision (ECCV) 2024*. –.
- [9] Jonathan Ho and Tim Salimans. 2022. Classifier-free diffusion guidance. *arXiv preprint arXiv:2207.12598* (2022).
- [10] Jie Hu, Yawen Huang, Yilin Lu, Guoyang Xie, Guannan Jiang, and Yefeng Zheng. 2024. AnomalyXFusion: Multi-modal Anomaly Synthesis with Diffusion. *arXiv preprint arXiv:2404.19444* (2024).
- [11] Teng Hu, Jiangning Zhang, Ran Yi, Yuzhen Du, Xu Chen, Liang Liu, Yabiao Wang, and Chengjie Wang. 2024. Anomalydiffusion: Few-shot anomaly image generation with diffusion model. In *Proceedings of the AAAI Conference on Artificial Intelligence (AAAI)*, Vol. 38. 8526–8534.
- [12] Chaoqin Huang, Aofan Jiang, Jinghao Feng, Ya Zhang, Xinchao Wang, and Yanfeng Wang. 2024. Adapting visual-language models for generalizable anomaly detection in medical images. In *Proceedings of the IEEE/CVF Conference on Computer Vision and Pattern Recognition (CVPR)*. 11375–11385.
- [13] Stepan Jezek, Martin Jonak, Radim Burget, Pavel Dvorak, and Milos Skotak. 2021. Deep learning-based defect detection of metal parts: evaluating current methods in complex conditions. In *2021 13th International congress on ultra modern telecommunications and control systems and workshops (ICUMT)*. IEEE, 66–71.
- [14] Diederik P Kingma. 2013. Auto-encoding variational bayes. *arXiv preprint arXiv:1312.6114* (2013).
- [15] Junnan Li, Dongxu Li, Silvio Savarese, and Steven Hoi. 2023. Blip-2: Bootstrapping language-image pre-training with frozen image encoders and large language models. In *International Conference on Machine Learning (ICML)*. 19730–19742.
- [16] Jiaqi Liu, Guoyang Xie, Jinbao Wang, Shangnian Li, Chengjie Wang, Feng Zheng, and Yaochu Jin. 2024. Deep industrial image anomaly detection: A survey. *Machine Intelligence Research* 21, 1 (2024), 104–135.
- [17] I Loshchilov. 2017. Decoupled weight decay regularization. *arXiv preprint arXiv:1711.05101* (2017).
- [18] Alex Nichol, Prafulla Dhariwal, Aditya Ramesh, Pranav Shyam, Pamela Mishkin, Bob McGrew, Ilya Sutskever, and Mark Chen. 2021. Glide: Towards photorealistic image generation and editing with text-guided diffusion models. *arXiv preprint arXiv:2112.10741* (2021).
- [19] Shuanlong Niu, Bin Li, Xinggang Wang, and Hui Lin. 2020. Defect image sample generation with GAN for improving defect recognition. *IEEE Transactions on Automation Science and Engineering* 17, 3 (2020), 1611–1622.
- [20] Utkarsh Ojha, Yijun Li, Jingwan Lu, Alexei A Efros, Yong Jae Lee, Eli Shechtman, and Richard Zhang. 2021. Few-shot image generation via cross-domain correspondence. In *Proceedings of the IEEE/CVF Conference on Computer Vision and Pattern Recognition (CVPR)*. 10743–10752.
- [21] Utkarsh Ojha, Yijun Li, Jingwan Lu, Alexei A Efros, Yong Jae Lee, Eli Shechtman, and Richard Zhang. 2021. Few-shot image generation via cross-domain correspondence. In *Proceedings of the IEEE/CVF Conference on Computer Vision and Pattern Recognition (CVPR)*. 10743–10752.
- [22] Patrick von Platen, Suraj Patil, Anton Lozhkov, Pedro Cuenca, Nathan Lambert, Kashif Rasul, Mishig Davaadorj, and Thomas Wolf. 2022. Diffusers: State-of-the-art diffusion models. <https://github.com/huggingface/diffusers>.
- [23] Alec Radford, Jong Wook Kim, Chris Hallacy, Aditya Ramesh, Gabriel Goh, Sandhini Agarwal, Girish Sastry, Amanda Askell, Pamela Mishkin, Jack Clark, et al. 2021. Learning transferable visual models from natural language supervision. In *International Conference on Machine Learning (ICML)*. PMLR, 8748–8763.
- [24] Aditya Ramesh, Prafulla Dhariwal, Alex Nichol, Casey Chu, and Mark Chen. 2022. Hierarchical text-conditional image generation with clip latents. *arXiv preprint arXiv:2204.06125* 1, 2 (2022), 3.
- [25] Robin Rombach, Andreas Blattmann, Dominik Lorenz, Patrick Esser, and Björn Ommer. 2022. High-resolution image synthesis with latent diffusion models. In *Proceedings of the IEEE/CVF Conference on Computer Vision and Pattern Recognition (CVPR)*. 10684–10695.
- [26] Olaf Ronneberger, Philipp Fischer, and Thomas Brox. 2015. U-net: Convolutional networks for biomedical image segmentation. In *Medical image computing and computer-assisted intervention (MICCAI)*. Springer, 234–241.
- [27] Chitwan Saharia, William Chan, Saurabh Saxena, Lala Li, Jay Whang, Emily L Denton, Kamyar Ghasemipour, Raphael Gontijo Lopes, Burcu Karagol Ayan, Tim Salimans, et al. 2022. Photorealistic text-to-image diffusion models with deep language understanding. *Advances in Neural Information Processing Systems (NeurIPS)* 35 (2022), 36479–36494.
- [28] Tim Salimans, Ian Goodfellow, Wojciech Zaremba, Vicki Cheung, Alec Radford, and Xi Chen. 2016. Improved techniques for training gans. *Advances in Neural Information Processing Systems (NeurIPS)* 29 (2016).
- [29] Han Sun, Yunkang Cao, and Olga Fink. 2024. CUT: A Controllable, Universal, and Training-Free Visual Anomaly Generation Framework. *arXiv preprint arXiv:2406.01078* (2024).
- [30] Zeyue Xue, Guanglu Song, Qishan Guo, Boxiao Liu, Zhuofan Zong, Yu Liu, and Ping Luo. 2024. Raphael: Text-to-image generation via large mixture of diffusion paths. *Advances in Neural Information Processing Systems (NeurIPS)* 36 (2024).
- [31] Hu Ye, Jun Zhang, Sibo Liu, Xiao Han, and Wei Yang. 2023. Ip-adapter: Text compatible image prompt adapter for text-to-image diffusion models. *arXiv preprint arXiv:2308.06721* (2023).
- [32] Vitjan Zavrtanik, Matej Kristan, and Danijel Skočaj. 2021. Draem-a discriminatively trained reconstruction embedding for surface anomaly detection. In *Proceedings of the IEEE/CVF international conference on computer vision (ICCV)*. 8330–8339.
- [33] Gongjie Zhang, Kaiwen Cui, Tzu-Yi Hung, and Shijian Lu. 2021. Defect-GAN: High-fidelity defect synthesis for automated defect inspection. In *Proceedings of the IEEE/CVF Winter Conference on Applications of Computer Vision (WACV)*. 2524–2534.
- [34] Hui Zhang, Zuxuan Wu, Zheng Wang, Zhineng Chen, and Yu-Gang Jiang. 2023. Prototypical residual networks for anomaly detection and localization. In *Proceedings of the IEEE/CVF Conference on Computer Vision and Pattern Recognition (CVPR)*. 16281–16291.
- [35] Lymni Zhang, Anyi Rao, and Maneesh Agrawala. 2023. Adding conditional control to text-to-image diffusion models. In *Proceedings of the IEEE/CVF International Conference on Computer Vision (ICCV)*. 3836–3847.
- [36] Ximiao Zhang, Min Xu, and Xiuzhuang Zhou. 2024. RealNet: A feature selection network with realistic synthetic anomaly for anomaly detection. In *Proceedings of the IEEE/CVF Conference on Computer Vision and Pattern Recognition (CVPR)*. 16699–16708.
- [37] Shihao Zhao, Dongdong Chen, Yen-Chun Chen, Jianmin Bao, Shaozhe Hao, Lu Yuan, and Kwan-Yee K Wong. 2023. Uni-controlnet: All-in-one control to text-to-image diffusion models. *Advances in Neural Information Processing Systems (NeurIPS)* 36 (2023).
- [38] Shengyu Zhao, Zhijian Liu, Ji Lin, Jun-Yan Zhu, and Song Han. 2020. Differentiable augmentation for data-efficient gan training. *Advances in Neural Information Processing Systems (NeurIPS)* 33 (2020), 7559–7570.
- [39] Yang Zou, Jongheon Jeong, Latha Pemula, Dongqing Zhang, and Onkar Dabeer. 2022. Spot-the-difference self-supervised pre-training for anomaly detection and segmentation. In *European Conference on Computer Vision (ECCV)*. Springer, 392–408.

A Implementation Details

A.1 Dataset

The MVTec AD dataset consists of 5,354 images across 15 categories for industrial anomaly detection tasks. These categories include 10 object categories and 5 texture categories. Each category is represented by defect-free training images and a test set containing both defect-free and defective images. Pixel-level annotations are provided for all anomalies in this dataset. We utilized the captions from MVTec AD Caption [10] for training and testing, which were carefully designed to ensure cross-modal complementarity.

The MPDD dataset includes 1,346 images from 6 types of industrial metal products, each captured under varying lighting conditions and non-uniform backgrounds. This dataset features multiple products in each image, with diverse placement orientations, shooting distances, and positions, making it a challenging dataset for anomaly detection. The text descriptions provided for each image consist of the product types and the specific anomaly categories identified.

The ViSA dataset comprises 9,621 normal images and 1,200 anomaly images across 12 categories. The dataset includes categories with complex structures, such as PCBs, and categories that require the detection of multiple objects, such as capsules. These characteristics make it a challenging dataset for both anomaly detection and localization tasks, requiring high precision to accurately identify and classify the anomalies. The text descriptions are directly provided by the dataset.

While some anomalies are difficult to describe, our method considers this limitation by incorporating image reference prompts in addition to text descriptions. The image reference prompt provides a visual example of the anomaly type, enabling our model to synthesize realistic anomalies even when textual descriptions are ambiguous.

A.2 Mask Generation

Given the limited number of real anomaly masks in the dataset and the lack of diversity in mask data even after augmentation, we adopt a method similar to AnoDiff [11] to generate additional anomaly masks by learning the distribution of real anomaly masks. Specifically, we use the textual inversion technique [7] to learn a mask embedding e_m , which serves as a text condition for generating diverse anomaly masks.

Initially, the mask embedding e_m is composed of randomly initialized tokens, which are then optimized by minimizing the following objective function:

$$e_m^* = \arg \min_{e_m} \mathbb{E}_{z \sim \mathcal{E}(m), \epsilon, t} [\|\epsilon - \epsilon_\theta(z_t, t, e_m)\|_2^2].$$

Once trained, the mask embedding is used as a text condition to guide the generation process within a latent diffusion model (LDM) [25]. We employ classifier-free guidance [9] to adjust the influence of the mask embedding, as follows:

$$\hat{\epsilon}_\theta(x_t | e_m) = \epsilon_\theta(x_t) + s \cdot (\epsilon_\theta(x_t, e_m) - \epsilon_\theta(x_t)),$$

where s is a scaling factor controlling the strength of the text guidance. Following the setup in textual inversion, s is set to 5 to ensure that the generated masks accurately capture anomaly-specific features and positional diversity.

Algorithm 2: Feature Extraction with Caching in CSM

Data: Visual anomaly descriptor I_a , textual anomaly descriptor T_a , anomaly region mask M_A

Input: Cache directory $cache_dir$, where cache files are stored in the format $cache_dir/I_a.pt$

Output: Extracted cross-modal semantic feature F_c

```

cache_file = cache_dir/I_a.pt if cache_file exists then
  F_c = load(cache_file)
else
  Extract features F_c = ExtractFeatures(I_a, T_a, M_A)
  Save the extracted features F_c to cache_file
return F_c

```

A.3 Feature Extraction with Caching in CSM

In Cross-modal Semantic Modeling (CSM), the Visual-Language Model is frozen, and the trainable attention guidance variable e_g is used to guide the VLM in generating cross-modal semantic features that focus more on the anomaly region. Since we do not train the VLM, the extracted features remain fixed when the input is fixed. This design brings a potential benefit: once these features are extracted for the first time during training, they can be cached. As shown in Algorithm 2, in subsequent training steps, whenever these features are needed, they can be loaded directly from the cache, avoiding the need for recomputation. This not only eliminates the overhead of recalculating image and text features but also significantly speeds up the training process of AnomalyControl. This approach saves substantial computational resources and time, improving the overall training efficiency.

A.4 Training Details

We use the AdamW optimizer [17] with a fixed learning rate of 0.0001 and weight decay of 0.01. For classifier-free guidance, text or cross-modal semantic features are independently dropped with a probability of 0.05, and both are dropped simultaneously with a probability of 0.05. Training is conducted on a single A100 GPU, requiring approximately three days for 200K iterations. During inference, a 30-step DDIM sampler is used, with a guidance scale of 7.5, to achieve a balance between fidelity and generalization in the generated anomalies.

B More Quantitative experiments

Table 5 presents the generation quantitative results on the MPDD and ViSA datasets, where the Inception Score (IS) and Intra-cluster Pairwise Learned Perceptual Image Patch Similarity (IL) are used to evaluate the quality and diversity of the generated anomalies. Our method outperforms existing SOTA models (DFMGAN and AnoDiff) in both datasets, demonstrating superior generation quality. Specifically, on the MPDD dataset, our approach achieves the highest IS of 1.71 and IL of 0.47, while on the ViSA dataset, it reaches an IS of 1.65 and IL of 2.12, surpassing the performance of other methods.

Table 6 further demonstrates our method's robustness by providing anomaly detection results on the MVTec AD, MPDD, and ViSA datasets. This table includes the anomaly detection results for

Table 6: Results of anomaly detection on three datasets. “-P” denotes the results of anomaly localization (pixel-level) and “-I” denote the results of anomaly detection (image-level).

MVTec AD						
Object	AUC-P	AP-P	F1-P	AUC-I	AP-I	F1-I
capsule	98.9	72.9	62.5	99.5	99.1	95.9
bottle	99.5	93.0	92.4	100	100	100
carpet	99.4	74.1	73.9	97.7	99.4	94.4
leather	99.8	79.9	74.1	100	100	99.2
pill	99.8	96.4	90.0	98.3	99.6	97.4
transistor	99.6	94.4	87.2	100	100	100
tile	99.5	94.5	89.0	100	100	100
cable	99.2	87.8	86.3	99.8	99.8	98.4
zipper	99.6	86.8	78.6	100	100	100
toothbrush	99.5	81.7	80.1	100	100	100
metal nut	99.7	98.3	93.3	99.9	100	99.2
hazelnut	99.7	96.1	89.8	99.9	100	99.0
screw	99.4	86.6	80.1	95.1	99.5	91.7
grid	98.9	68.8	59.2	99.5	99.1	98.7
wood	99.8	99.3	82.2	99.7	99.9	98.8
MEAN	99.5	87.4	81.2	99.3	99.8	98.0
MPDD						
Object	AUC-P	AP-P	F1-P	AUC-I	AP-I	F1-I
bracket black	95.4	30.6	35.5	98.5	82.5	80.9
bracket white	95.2	31.7	38.5	98	83.2	81.1
bracket brown	96.2	36.7	33.3	96.6	83.4	82.8
connector	95.9	64	54.5	100	100	100
metal plate	99.5	87.4	88.2	100	100	100
tubes	96.6	53.4	57.5	97.3	93.8	89.9
MEAN	96.5	50.6	51.2	98.4	90.5	89.1
VisA						
Object	AUC-P	AP-P	F1-P	AUC-I	AP-I	F1-I
pcb1	99.5	51.2	55.4	97.8	95.5	95.1
pcb2	100	40.4	48.9	96.8	94.3	91.2
pcb3	99.3	47.1	52.9	98.2	95.5	95.7
pcb4	98	34.4	42.3	97.1	100	100
macaroni1	100	34.8	30.3	96.6	100	93.7
macaroni2	98.9	30.1	39.7	95.5	95.1	93.8
capsules	96.9	34.2	33.2	96.7	100	92.3
candle	99.3	16.3	26.4	95.2	97.9	73
cashew	97.6	15.8	22.3	97.2	95.4	93.4
chewinggum	100	74	79.1	97.8	97.5	100
fryum	99.3	43	50.3	93.9	97.1	95.9
pipe fryum	99.3	88.1	95.3	98.4	98.4	97.9
MEAN	99.0	42.5	48.0	96.8	97.2	93.5

Table 5: Generation quantitative results on MPDD and VisA datasets.

Dataset	DFMGAN		AnoDiff		Ours	
	IS	IL	IS	IL	IS	IL
MPDD	1.31	0.31	1.60	0.43	1.71	0.47
VisA	1.26	1.12	1.45	1.73	1.65	2.12

each anomaly object on these datasets, both at the pixel level (AUC-P, AP-P, F1-P) and image level (AUC-I, AP-I, F1-I). Our method consistently delivers high performance across all datasets, with particularly strong results in MVTec AD, where it achieves a mean F1-P of 81.2 and F1-I of 98.0. Additionally, our method shows impressive performance on both the MPDD and ViSA datasets, with a mean F1-I of 89.1 on MPDD and 93.5 on ViSA. These results underscore the effectiveness of our approach in detecting and localizing anomalies across various datasets and anomaly types. This effectiveness is attributed to the higher quality of the anomalies generated by our method, which provides more realistic and diverse training data for anomaly detection tasks.

C More Qualitative experiments

C.1 Generalization and Controllability in Anomaly Synthesis

As shown in Figure 1 (right examples) and Figure 4(b), our method effectively generalizes to unseen anomaly types using text-image reference prompts for flexible and controllable synthesis. We further demonstrate the generalization capability of our approach in Figure 7, where anomalies are synthesized on different materials (wood and leather) with various anomaly types (such as red stains and holes). These examples highlight our method’s flexibility in generating diverse anomalies, even beyond the training distribution. The key advantage of our approach is its ability to synthesize diverse and realistic anomalies beyond the training distribution, providing varied training data for detection tasks.

C.2 Anomaly Synthesis Across Diverse Datasets

In Figure 8 and Figure 9, we demonstrate additional examples of anomaly synthesis on the MPDD and ViSA datasets, respectively. These results further showcase our model’s ability to handle diverse anomaly types and generate realistic anomalies even when faced with different datasets and industrial contexts. Even when confronted with varying textures, materials, and anomaly types across these datasets, our method consistently produces high-quality and contextually appropriate anomalies, proving its robustness and adaptability. These examples highlight the model’s generalization capability, ensuring its effectiveness across a wide range of real-world scenarios.

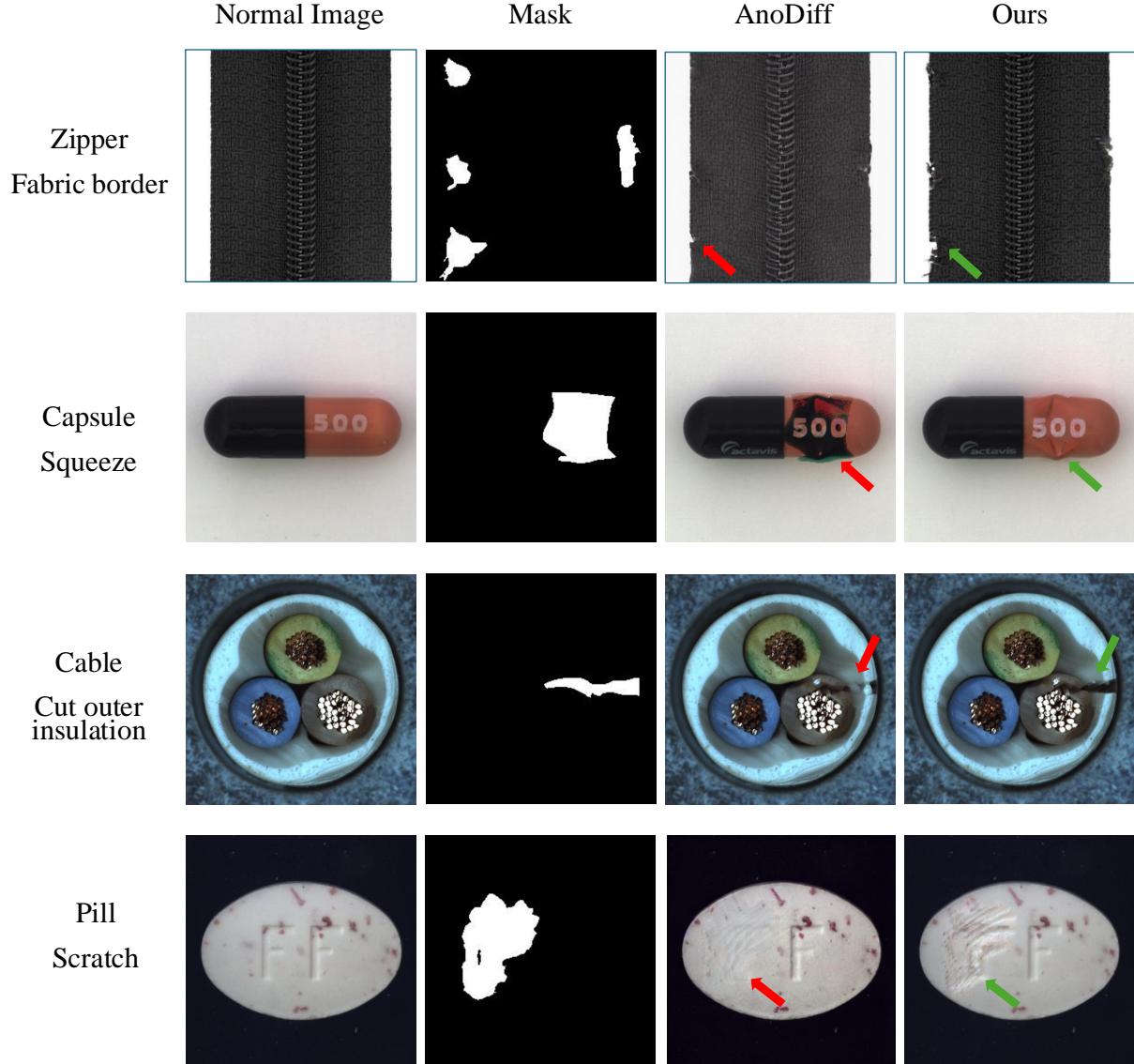


Figure 6: Comparison of anomaly synthesis results between AnoDiff and our method. The images show the same normal image (first column) and the same anomaly mask (second column), with the results generated by AnoDiff (third column) and our method (fourth column). In the “zipper” example, our method generates an anomaly that better fits the mask and is closer to the real anomaly, even capturing the details of the broken fibers. In the “capsule” example, our method successfully generates the squeezed capsule’s shape, while AnoDiff fails to synthesize the anomaly. In the “cable” example, AnoDiff produces an anomaly with the artifact, while our method generates a more realistic one. In the “pill” example, our method’s anomaly better matches the mask, whereas AnoDiff produces a blurred anomaly boundary.

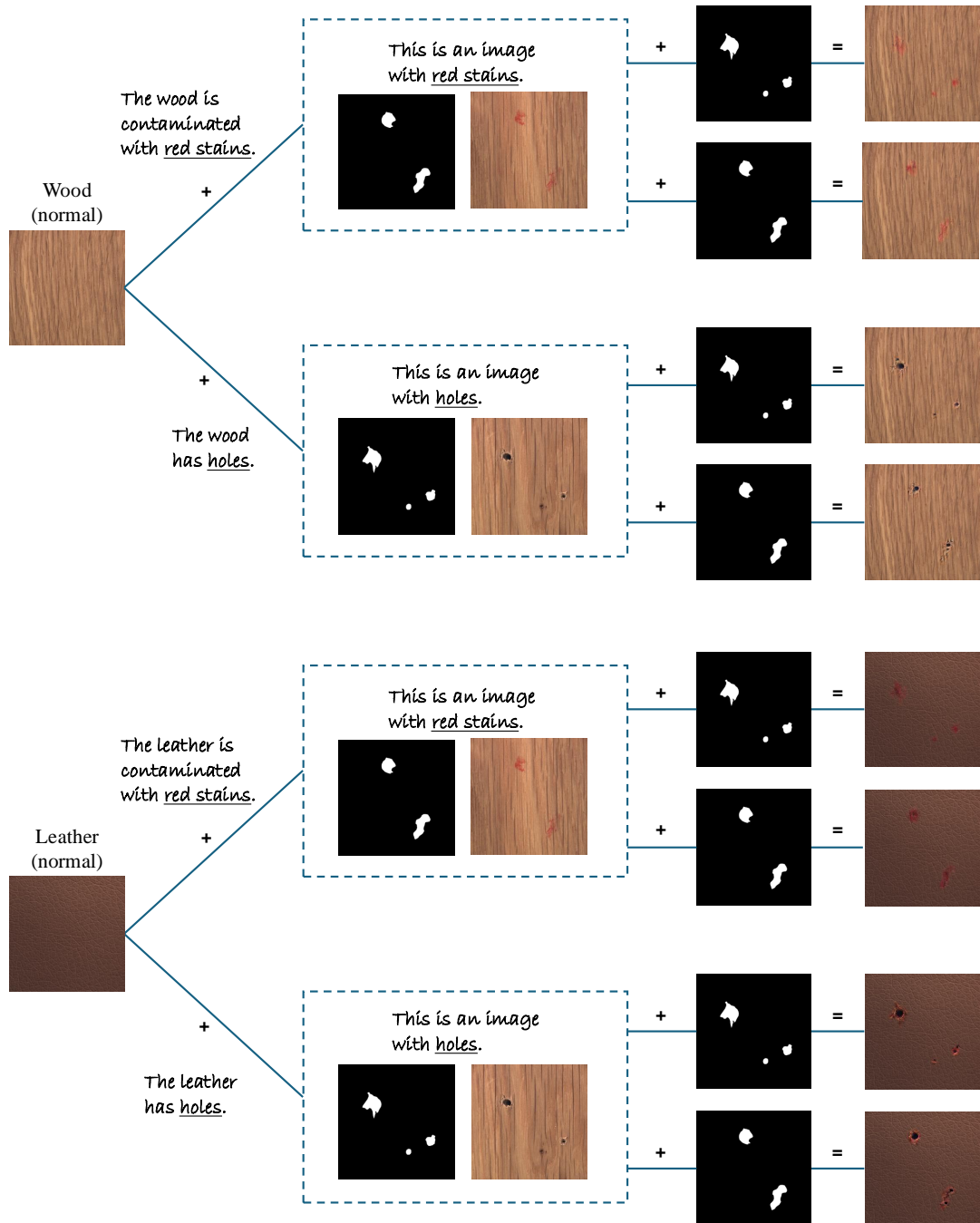


Figure 7: Controllable anomaly synthesis across different object categories and anomaly types. Given a normal image (wood or leather) and a text-image reference describing the desired anomaly (e.g., “red stains” or “holes”), our method synthesizes corresponding anomalies in the specified masked region. The anomaly type can be flexibly controlled via the reference, and it generalizes well across categories, demonstrating strong generalization capability.

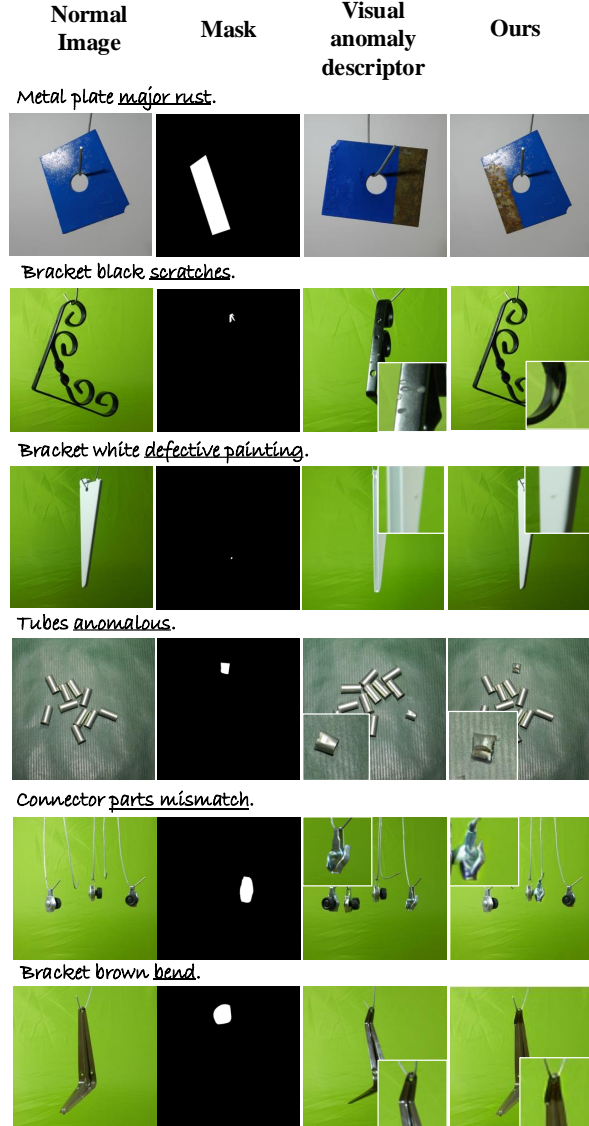


Figure 8: Display of anomaly synthesis on 6 objects from the MPDD dataset. The first column shows the normal image, the second column represents the mask area where anomalies need to be generated, the third column contains the visual anomaly descriptor providing visual guidance, and the fourth column displays the results generated by our method. Unlike simply copying the anomaly shown in the visual anomaly descriptor, our model predicts what the anomaly would look like in the given region indicated by the mask, considering the material and texture of the original normal image. The generated anomalies are consistent with the context of the image and are realistic in their appearance. Zoom in for better clarity and details.

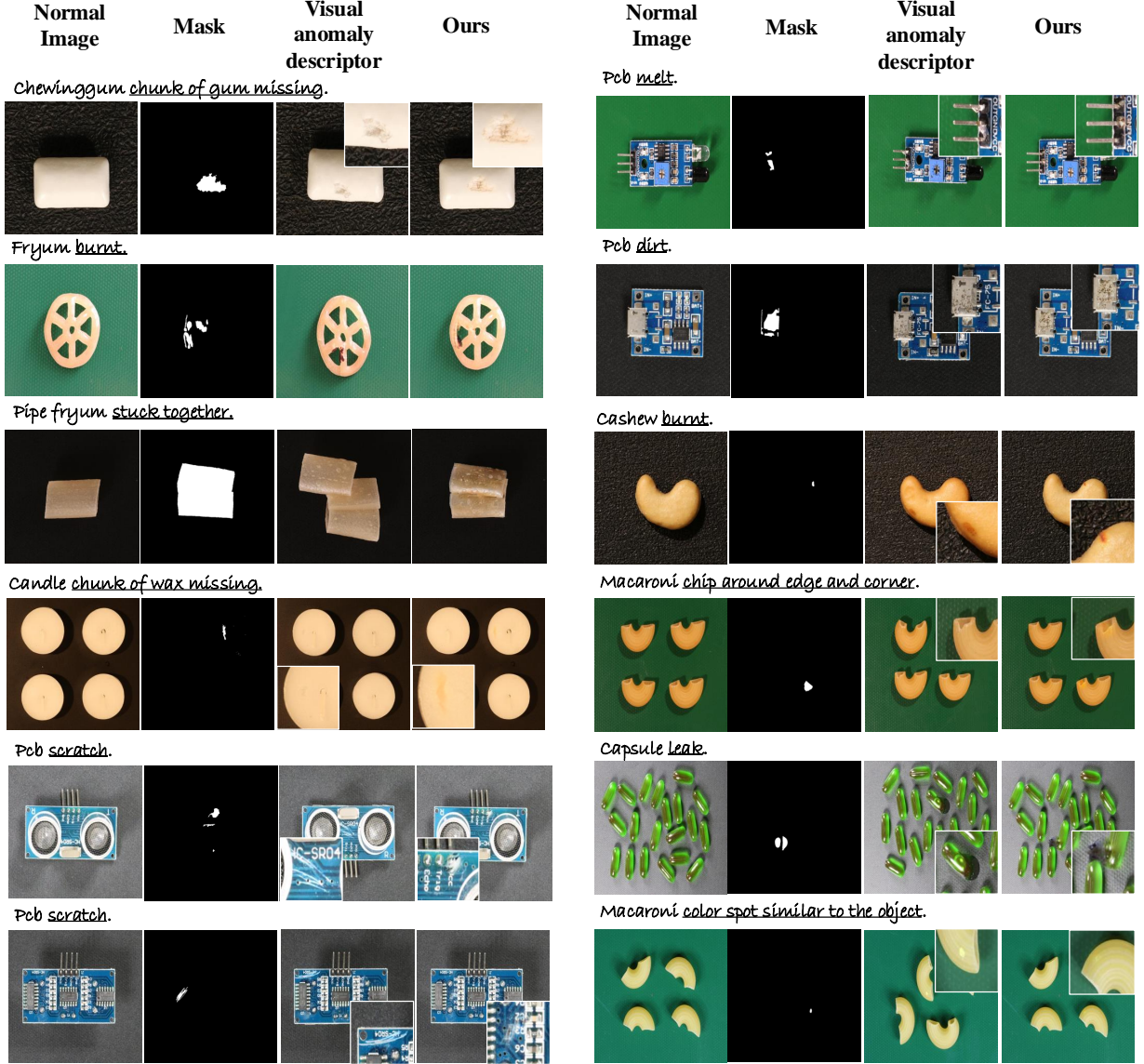


Figure 9: Display of anomaly synthesis on 12 objects from the ViSA dataset. The first column shows the normal image, the second column represents the mask area where anomalies need to be generated, the third column contains the visual anomaly descriptor providing visual guidance, and the fourth column displays the results generated by our method. Unlike simply copying the anomaly shown in the visual anomaly descriptor, our model predicts what the anomaly would look like in the given region indicated by the mask, considering the material and texture of the original normal image. The generated anomalies are consistent with the context of the image and are realistic in their appearance. Zoom in for better clarity and details.